UPGRADE OF THE CORNELL ELECTRON STORAGE RING AS A SYNCHROTRON LIGHT SOURCE*

D. L. Rubin, J. A. Crittenden, J. P. Shanks, S. Wang
CLASSE, Ithaca, NY, USA

Abstract

The planned upgrade of the Cornell Electron Storage Ring as an X-ray source for CHESS will include an increase in beam energy and decrease in emittance from 100 nm-rad at 5.3 GeV to 30 nm-rad at 6 GeV, increase in beam current from 120 to 200 mA, continuous top-off injection of the single circulating beam, and four new zero dispersion insertion straights that can each accommodate a pair of canted undulators. The existing sextant of the storage ring arc that serves as the source for all of the CHESS X-ray beam lines will be reconfigured with 6 double-bend achromats, each consisting of two pairs of horizontally focusing quadrupoles, and a single pair of combined-function gradient bend magnets. The chromaticity will be compensated by the existing sextupoles in the legacy FODO arcs. We describe details of the linear optics, sextupole distributions to maximize dynamic aperture and injection efficiency, and characterization of magnetic field and alignment error tolerance.

INTRODUCTION

The Cornell High Energy Synchrotron X-ray Source (CHESS) was originally developed to operate parasitically with the particle physics electron-positron colliding beam program at the Cornell Electron/Positron Storage Ring (CESR). X-ray beam lines were constructed to take advantage of radiation from both electron and positron beams in the sextant (the south arc) of the ring that is accessible. (The remainder of the ring circumference of 768 m is in an underground tunnel.) The lattice and layout of the south arc were designed to generate high luminosity. An upgrade is now underway to reconfigure the south arc for X-ray science. The plan is to replace the 100m arc [1] with six double-bend achromats and seven low-beta, zero-dispersion straights. Five of the straights will be equipped with undulator or wiggler insertion devices. All of the beam lines will be rearranged to intercept X-rays from a single clockwise beam, eliminating the complexity associated with two-beam operation [2]. The beam energy will be increased from 5.3 to 6 GeV. The horizontal emittance, heretofore limited by the FODO structure in the south arc and the lattice constraints imposed by two beam operation, will be reduced from 100 nm at 5.3 GeV to 30 nm at 6 GeV. The 13.7-m long achromats are compact. In order to save space for correction magnets and beam instrumentation, the vertical focusing in the achromat is derived from the field gradient in the bending magnets. Flexibility to tune and correct optics and orbits is provided by four independently powered horizontally focusing quadrupoles and horizontal and vertical dipole correctors. Matching of the achromat optics into the legacy FODO structure in the CESR arcs is accomplished with the addition of a single pair of quadrupoles in the transition region.

* Work supported by the National Science Foundation DMR 13-32208

LATTICE

The operational parameters of CHESS at present are compared to the new machine in Table 1. A comparison of pin-hole flux for CHESS, APS and the CHESS post-upgrade is shown in Fig. 1. With a 3.5 m undulator, pin-hole flux at CHESS will exceed that of APS with undulator A.

Table 1: CHESS and Post-upgrade Parameters

Parameter	Present CHESS	Post Upgrade
Particle beams	2 Counter-rotating	Single (clockwise)
Insertion devices	One pair undulators	Five pairs undulators
E_{beam} [GeV]	5.3	6.0
I_{beam} [mA]	125 X 125	200
Bunches	20 e^+ X 45 e^-	100
ϵ_x [nm]	100	30
ϵ_y [nm]	1	0.1 → 1
Injection	Top-off e^+/5 min Refill e^-/2 hrs	Top-off/3 min → const I

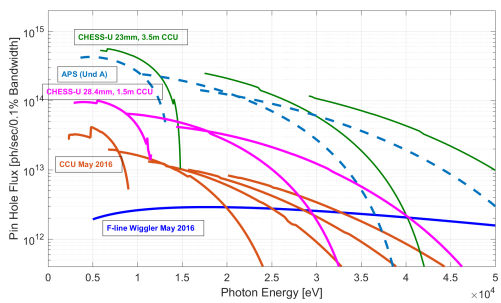

Figure 1: Pin-hole flux [photons/sec/0.1% Bandwidth]. Red lines are CHESS 1.5 m compact undulator May 2016. Purple - CHESS post-upgrade with 1.5 m compact undulator. Dashed blue - APS undulator A, and green - CHESS post-upgrade with 3.5 m undulator.

Achromat

The achromat shown in Fig. 2, consists of four horizontally focusing quadrupoles, and a pair of defocusing gradient bends. Beam parameters at midpoint of the ~4 meter straight are $\beta_x = 11.2$ m, $\beta_y = 2.6$ m and $\eta = 0$ m. β_x is limited from below by the separation of the quad (Q_1) at the end of the straight from the adjacent gradient-bend. If the zero-dispersion condition is relaxed by varying the quadrupole strengths, horizontal beta can be reduced to $\beta_x = 3.8$ m,

β_y = 2.7 m and η = 0.17 m or increased to $\beta_x \sim 25$ m. The 2.35 m long combined-function magnets have a gradient of -8.769 T/m and bending field of 0.64 T at 6-GeV beam energy.

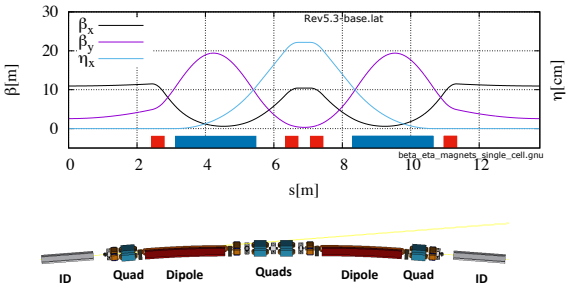

Figure 2: Double-bend achromat

Layout

The present and future layout of the south arc of the storage ring is shown in Fig. 3. There are five pairs of canted undulators in the new layout. Superconducting damping wigglers, essential for the CesrTA damping rings R&D program, are relocated to the straights between s=-30 m and s=-10 mm. The quadrupoles labeled Q09AW and Q09AE are added to facilitate the matching from the low dispersion achromats into the high dispersion FODO structure of the arcs.

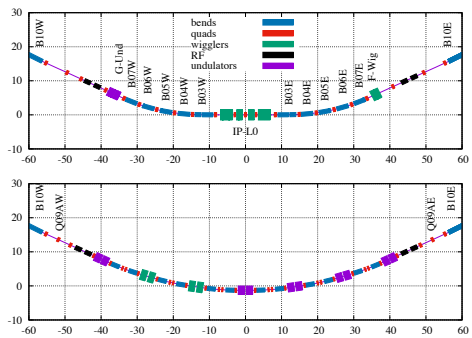

Figure 3: Legacy layout above and new layout below. After the upgrade, the single beam travels from right to left. The bending magnets B10E and B10W at the start and end of the legacy CESR arcs bound the sectors of the ring that remain unchanged.

Matching and Arc Lattice

The Twiss parameters of the full ring lattice are shown in Fig. 4. The south arc is bounded at each end by a pair of RF cavities. The four single-cell, superconducting 500 MHz cavities provide up to 8 MV accelerating voltage. Note that there is zero dispersion in the RF straights. Collimators at $s = \pm 335$ m shadow the narrow-gap insertion devices in the achromats from particles with large vertical amplitude that appear in the ring during injection. The lattice is designed with peak vertical beta in the collimators. The peak horizontal beta is at the injection point (s = 257 m). The limiting vertical aperture is the narrow-gap undulator

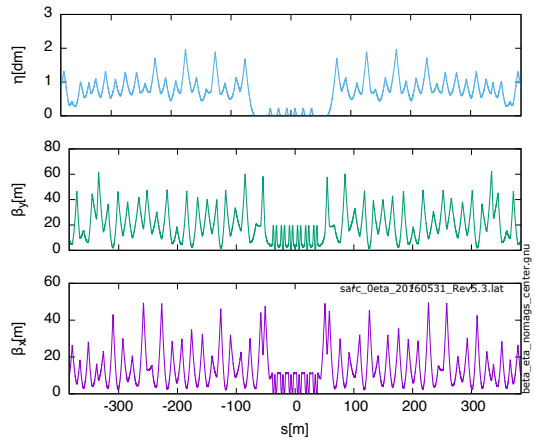

Figure 4: The six achromats that comprise the reconfigured south arc are at the center of the figure. The legacy FODO optics complete the ring lattice.

chambers (±2.3mm) in the insertion straights. The limiting horizontal aperture is at the injection point in the arc.

ENERGY APERTURE AND LIFETIME

The momentum compaction of the predominantly FODO optics is relatively large ($\alpha_p \sim 0.006$) and as a result the energy aperture, which scales as V_{RF}/α_p, is limited to less that 0.9% with V_{RF} = 8 MV. The effect of the narrow energy aperture is to reduce Touschek lifetime. Lifetime at 2 mA/bunch and 0.1% emittance coupling is estimated at 4 hours. Near constant beam current will be maintained with topoff every few minutes.

SEXTUPOLES

Chromaticity is compensated with sextupoles in the legacy FODO arcs, in order to take advantage of the relatively high dispersion. ($\langle\eta\rangle \sim 1$ m). Dispersion in the south arc is an order of magnitude smaller and local compensation would require very strong sextupoles. The sextupole distribution is designed in two steps: 1) Minimize the non-symplecticity of numerically computed Jacobian of the full turn map, the energy dependence of the trace of the full turn Jacobian; and energy dependence of the lattice β-functions; 2) Compute and minimize selected resonance-driving terms in the Hamiltonian, as well as chromatic β, second order dispersion and chromaticity and amplitude dependent tune.

ERROR TOLERANCE

Tolerance to field and alignment errors and design of emittance tuning algorithms, is complicated by the coupling of focusing and steering in the achromat combined-function magnets. Simulations are used to evaluate sensitivity to magnet field and alignment errors, and the procedure for measuring and compensating those errors. The study begins with introduction of misalignments and field errors into the design lattice. The distribution of magnet offset, roll, tilt, pitch and field errors is based on survey data. The measurement of lattice functions such as betatron amplitude and

phase, transverse coupling, dispersion and orbit depends on the quality of the beam position monitors (BPMs) [3]. To that end, BPM errors - offset, tilt, and gain are incorporated in the simulation of those measurements. Corrections are applied using steering dipoles and skew quads as well as all lattice quadrupoles and combined-function magnets. Corrector magnets and beam position monitors in the achromat are shown in Fig. 5a. The corrected lattice is characterized in terms of emittance, orbit and dispersion. The misalignment and correction procedure is evaluated with 100 random seeds. Histograms of vertical emittance for all of the seeds, at each iteration of the correction procedure are shown in Fig. 5b. For all 100 seeds β-functions are corrected to within 1% of design and vertical emittance to less than 10 pm-rad, corresponding to an emittance coupling of order 0.1%.

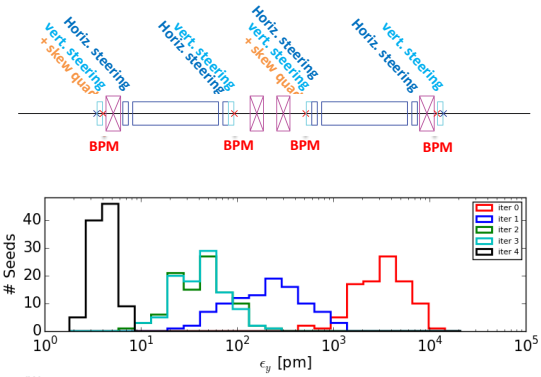

Figure 5: BPMs and corrector magnets (a-top) simulated vertical emittances after each iteration of correction algorithm (b-below).

DYNAMIC APERTURE

We characterize nonlinear dynamics with a frequency map. The map is based on scans of trajectories with starting amplitudes covering the x/y and x/δ planes in phase space. A tune shift for each trajectory is computed by comparing FFTs of the first and last 1024 turns. A representative frequency map is in Fig. 6. The sextupole distribution is designed according to the algorithm described earlier. The simulation includes guide field magnet and insertion device multipole errors as well as corrected misalignment and field errors. We assume that the insertion devices are Cornell compact undulators (CCU) [4] and that there is a CCU in each of the ten achromat straights. The CCU is an 104-pole, 1.5-m-long undulator with 7-mm gap between the pole tips and 0.95 T peak field. The transverse field roll-off and the measured field integrals are modeled as a 27-term sinusoidal expansion [5]. The dashed red line in the Fig. 6 indicates the projected physical aperture. Evidently non-linearity does not limit acceptance.

INJECTION

Injection into the storage ring is simulated to determine dependence of capture efficiency and particle losses on lattice nonlinearity, field errors and misalignments. Particles are launched at the injection point with 6D phase space

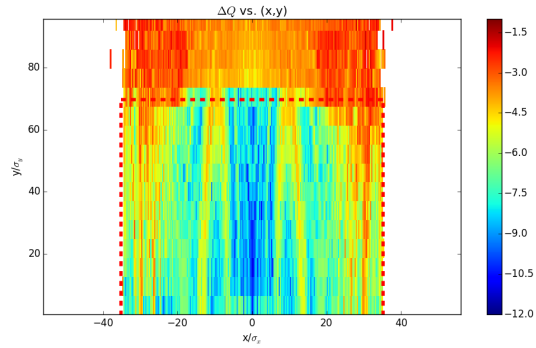

Figure 6: Frequency map, including guide-field and insertion-device multipole errors, and corrected field and alignment errors. Color corresponds to tune shift or diffusion rate.

typical for the injector. The centroid of the distribution is displaced x_{inj} = 22 mm from the closed orbit, consistent with measurements of injection into CESR. The 200-particle distribution is tracked for 400 turns. The simulation includes guide field magnet and insertion device multipole errors as well as corrected misalignment and field errors. Incorporated as part of tune scan, the simulation indicates (Fig. 7) a generous tune footprint where injection efficiency is in excess of 85% and losses into the insertion device undulators are much less than 1%(not shown). Additional gains are anticipated with planned improvements in the stability of the injected beam, and the matching from synchrotron through the transfer line and into the ring.

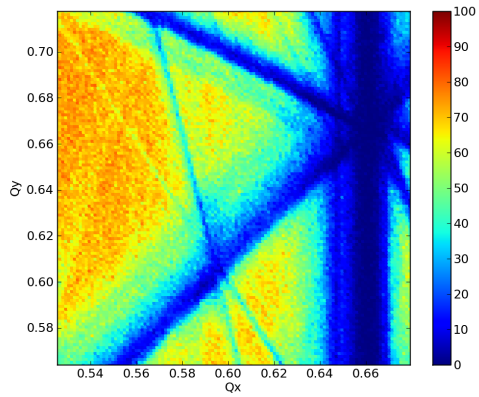

Figure 7: Injection tune scan including multipoles, misalignments and 10 undulators. Color code is efficiency.

CONCLUSION

The sextant of the CESR that serves the CHESS X-ray community will be reconfigured with 6 double-bend achromats creating seven zero-dispersion straights. Five of the straights will be outfitted with canted insertion devices and the remaining two with superconducting damping wigglers. The beam energy will increase to 6 GeV from 5.3 GeV, the horizontal emittance be reduced from 100 nm to 30 nm and the single-beam current will increase from 120 to 200 mA. Commissioning will begin in late 2018.

REFERENCES

[1] D.L. Rubin, Y. Li, A.A. Mikhailichenko, and S. Wang, "CESR Low Emittance Upgrade with Combined Function Bends" in *IPAC2013: Proceedings of the 4th International Particle Accelerator Conference, Shanghai, China*, Z. Dai *et al.*, Eds., JACoW (2013), p. 1719-1721.

[2] R. Littauer, *IEEE Trans. Nucl. Sci.* NS-32 (1985) 1610.

[3] J.P. Shanks, D. L. Rubin, and D. C. Sagan, "Low-Emittance Tuning at the Cornell Electron Storage Ring Test Accelerator," *Phys. Rev. ST Accel. Beams* **17**, 044003 (Apr. 2014).

[4] A. Temnykh *et al.*, "Compact Undulator for the Cornell High Energy Synchrotron Source: Design and Beam Test Results" in *SRI 2012:Proceedings of the 11th International Conference on Synchrotron Radiation Instrumentation*, Lyon, France (2013), 425, 032004.

[5] S. Wang, D.L. Rubin, and J.P. Shanks, "CESR Lattice for Two Beam Operations with Narrow Gap Undulators at CHESS", in *IPAC2016: Proceedings of the 7th International Particle Accelerator Conference*, Busan, Korea (2016), Paper WEPOW053.